Long non-coding RNA LINC00473 acts as a microRNA-29a-3p sponge to promote hepatocellular carcinoma development by activating Robo1-dependent PI3K/AKT/mTOR signaling pathway

Qiqin Song, Hongyue Zhang, Jinan He, Hongyan Kong, Ran Tao, Yu Huang, Haijing Yu, Zhongwei Zhang, Zhiyong Huang, Lai Wei, Chenghai Liu, Likui Wang, Qin Ning and Jiaquan Huang

Ther Adv Med Oncol

2020, Vol. 12: 1–21

DOI: 10.1177/1758835920937890

Abstract

Background: Long non-coding RNAs have suppressive or oncogenic effects in various types of cancers by serving as competing endogenous RNAs for specific microRNAs. In the present study, we aim to delineate the underlying mechanism by which the LINC00473/miR-29a-3p/Robo1 axis affects cell proliferation, migration, invasion, and metastasis in hepatocellular carcinoma (HCC).

Methods: The level of Robo1 was examined in HCC tissues and cells, along with its regulatory effects on proliferation, migration, and invasion of HCC cells. Afterwards, the possible involvement of the PI3K/AKT/mTOR signaling pathway was determined. Next, miR-29a-3p expression was overexpressed or inhibited to investigate its regulatory role on HCC cell activities. The interaction among miR-29a-3p, Robo1, and LINC00473 was further characterized. Finally, a xenograft tumor in nude mice was conducted to measure tumorigenesis and metastasis *in vivo*.

Results: miR-29a-3p was downregulated while Robo1 was upregulated in HCC tissues and cells. miR-29a-3p targeted Robo1 and negatively regulated its expression. In response to miR-29a-3p overexpression, Robo1 silencing or LINC00473 silencing, HCC cell proliferation, migration, invasion, tumor progression, and metastasis were impeded, which was involved with the inactivation of the PI3K/AKT/mTOR signaling pathway. Notably, LINC00473 could competitively bind to miR-29a-3p to upregulate Robo1 expression.

Conclusion: LINC00473 might be involved in HCC progression by acting as a miR-29a-3p sponge to upregulate the expression of Robo1 that activates the PI3K/AKT/mTOR signaling pathway, which leads to enhanced cell proliferation, migration, invasion, tumor progression, and metastasis in HCC.

Keywords: hepatocellular carcinoma, invasion, LINC00473, microRNA-29a-3p, migration, PI3K/AKT/mTOR signaling pathway, proliferation, Robo1

Received: 7 March 2019; revised manuscript accepted: 22 May 2020.

Correspondence to:
Jiaquan Huang
Department and Institute of Infection Disease, Tongji Hospital, Tongji Medical College, Huazhong University of Science Technology, No. 1095 JieFang Avenue, Wuhan 430030, Hubei Province, P. R. China
Huangjiaquan21@aliyun.com

Qiqin Song
Jinan He
Hongyan Kong
Ran Tao
Yu Huang
Haijing Yu
Zhongwei Zhang
Qin Ning
Department and Institute of Infectious Disease, Tongji Hospital, Tongji Medical College, Huazhong University of Science and Technology, Wuhan, Hubei, P. R. China

Hongyue Zhang
Department and Institute of Infectious Disease, Tongji Hospital, Tongji Medical College, Huazhong University of Science and Technology, Wuhan, Hubei, P. R. China

Department of Nephrology, Xiangyang Central Hospital, The Affiliated Hospital of Hubei University of Arts and Science, Xiangyang, Hubei, P. R. China

Zhiyong Huang
Department of Hepatobiliary Surgery, Tongji Hospital, Tongji Medical College, Huazhong University of Science and Technology, Wuhan, Hubei, P. R. China

Lai Wei
Department of Organ Transplant, Tongji Hospital, Tongji Medical College, Huazhong University of Science and Technology, Wuhan, Hubei, P. R. China

Chenghai Liu
Institute of Liver Disease, Shuguang Hospital, Shanghai University

Introduction

Hepatocellular carcinoma (HCC) is a malignancy of the liver and is known to be a fatal type of liver cancer, accounting for approximately 30% of all malignancies.[1] According to the World Health Organization, there are about 56,400 new cases of HCC reported annually worldwide, with the highest incidence in developing countries.[2] Several

of Traditional Chinese Medicine, Shanghai, P. R. China

Likui Wang
Savaid Medical School, University of Chinese Academy of Science Institute of Microbiology, Chinese Academy of Sciences, Beijing, P. R. China

predisposing factors responsible for the development of HCC include hepatitis virus infection (esp. hepatitis B or C viruses), alcohol abuse, and exposure to aflatoxin in food.[3] Despite significant advancements in therapeutic approaches for HCC, such as surgery and chemotherapy, HCC still shows a poor prognosis and high metastatic tendency.[4] Thus, it is essential to explore the underlying molecular mechanisms regarding the tumorigenesis of HCC.[5]

Long non-coding RNAs (lncRNAs) have been found to play promising roles in the prevention, early detection, diagnosis and treatment of HCC.[6] For example, lncRNA LINC00473 is amplified in HCC tissue and is associated with the accelerated proliferation and invasion of HCC cells, indicating its potential role in HCC treatment.[7] In addition to that, lncRNA LINC00473 functions as an oncogene in colorectal cancer and its depletion impairs tumor cell vitality, colony formation, and the ability of migration or invasion.[8] lncRNAs act as competing endogenous RNAs (ceRNAs) for specific microRNAs (miRNAs or miRs) and regulate functions of miRNAs as well as their target gene expression, thereby affecting HCC development.[9,10] A bioinformatics website available at http://www.microrna.org predicted a binding site between lncRNA LINC00473 and miR-29a-3p. The dysregulation of several miRNAs has been linked with underlying pathophysiology of various human malignancies, including HCC.[11] miR-29a-3p has recently been in the spotlight as a tumor suppressor whose encoding gene is frequently suppressed in cancers; one study reveals its ability to inhibit HCC cell migration and proliferation by decreasing expression of insulin-like growth factor 1 receptor.[12] Furthermore, miR-29a-3p has a suppressive role in the development of gastric cancer and its downregulation has been linked to the growth, migration, and invasion of gastric cancer cells.[13] The biological prediction and dual luciferase reporter gene assay results revealed that miR-29a-3p targeted roundabout homolog 1 (Robo1). Robo1 belongs to immunoglobulin superfamily and is cleaved by gamma-secretase and metalloproteinases, which can metastasize to the cell nucleus of cancer.[14] Robo1 is a prominent molecular barrier for tumor cells to obtain an invasive phenotype in prostate cancer.[15] A previous study suggested that Robo1 participates in the progression of HCC and can serve as a promising predictor for the prognosis of the disease.[16] Inhibition of Robo1 has been shown to prevent the formation of gastrointestinal vascular malformation by blocking the phosphoinositide-3 kinase (PI3K)/protein kinase B (AKT) signaling pathway.[17] The PI3K/AKT/mammalian target of rapamycin (mTOR) signaling pathway is mainly involved in the progression and treatment of cancers.[18] Another study showed an increased activation of the PI3K/AKT/mTOR signaling pathway in almost half of the HCC cases included in the study.[19] Based on the previously mentioned findings, we hypothesized that the possible interaction between LINC00473, miR-29a-3p, Robo1 and the PI3K/AKT/mTOR signaling pathway might affect the progression of HCC. Thus, the present study was conducted to clarify the potential roles of LINC00473 and miR-29a-3p in regulating HCC cell behaviors, with aims of identifying a therapeutic target to prevent HCC progression.

Methods

Ethical statement

The current study was conducted in strict accordance with the Declaration of Helsinki and approved by the Institutional Review Board of Tongji Hospital, Tongji Medical College, Huazhong University of Science and Technology (No. 201112005). Written informed consent was obtained from each participant prior to sample collection. Animal experiments were approved by the Ethnic Committee of Tongji Medical College, Huazhong University of Science and Technology (No. 201304002) and performed in strict accordance with the standard of the Guide for the Care and Use of Laboratory Animals published by the Ministry of Science and Technology of the People's Republic of China in 2006.

Study subjects

HCC tissues and paracancerous tissues were collected from 108 patients pathologically confirmed with HCC at the Tongji Hospital, Tongji Medical College, Huazhong University of Science and Technology from January 2012 to January 2013. There were 90 male patients and 18 female patients with the mean age of 50.21 ± 7.47 years. Among these patients, 18 of them (11 males and 7 females, aged 24–62 years, with a mean age of 45 ± 9.50 years) were recruited for experiments to detect the relevant expression in their clinical samples and paracancerous tissue samples. The 90 HCC cases included 11 cases with extrahepatic metastases, 76 with tumor recurrence, and 64 cases of intrahepatic recurrence. In addition,

all 90 patients with HCC (Table 1) had regular follow-up visits and regular monitoring, which lasted until January 2018, for a mean duration of 30.5 months (1–60 months). If tumor recurrence was detected, computed tomography scan or magnetic resonance imaging was conducted. The tumors were pathologically classified according to the guidelines of the International Union Against Cancer (UICC). All clinical specimens were collected from Tongji Hospital, Tongji Medical College, Huazhong University of Science and Technology (Wuhan, Hubei, China). The tissue samples were immediately frozen at –80°C following surgery.

Cell culture

Human HCC cell lines HepG2, Huh7, HCCLM3 and SK-Hep-1 and immortalized human liver cell line L02 purchased from China Center for Type Culture Collection of Wuhan University (Wuhan, Hubei, China) were cultured in Dulbecco's modified Eagle's medium (DMEM, Gibco, Germany, Grand Island, NY, USA) conjugated with 10% fetal bovine serum (FBS, Gibco, Germany, Grand Island, NY, USA) with 5% CO_2 at 37°C.

Lentiviral vector transduction

Lentivirus (LV)-miR-29a-3p, LV-negative control (NC), miR-29a-3p-Sponge, LV-Sponge, LV-Robo1, LV-Con, LV-short hairpin RNA (sh)-Robo1, LV-shCon, LV-sh-NC, and LV-shLINC00473 were purchased from Shanghai Genechem Co., Ltd. (Shanghai, China). Lentivirus overexpression vector was LV5 [EF-1a promoter, conjugated with green fluorescent protein (GFP)], and lentivirus shRNA vector with pGLVH1 (cytomegalovirus promoter, conjugated with GFP) (Shanghai Genechem Co., Ltd., Shanghai, China). LV-miR-29a-3p, LV-NC, LV-Robo1 and LV-Con were transduced into LV5, while LV-Sponge, miR-29a-3p-Sponge, LV-sh Robo1, LV-shCon, LV-sh-NC, and LV-shLINC00473 were transduced into pGLVH1.

Reverse transcription quantitative polymerase chain reaction (RT-qPCR)

Following total RNA extraction from cells and tissues with the use of the Trizol kit (Invitrogen, Carlsbad, CA, USA), reverse transcription was performed to synthesize first-strand complementary DNA (cDNA) using Transcript RT Kit (Tiangen Biotech, Beijing, China). The relative expression levels of miR-29a-3p, Robo1, and LINC00473 were detected using the TaqMan Human MiRNA Assay kit (GeneCopoeia, Guangzhou, China) and the SYBR Premix Ex TaqTM Kit (Takara, Shiga, Japan). U6 was considered as the internal control for miR-29a-3p, while glyceraldehyde-3-phosphate dehydrogenase (GAPDH) was regarded as a loading control for Robo1 and LINC00473. The primers for miR-29a-3p, Robo1, LINC00473, U6, and GAPDH were synthesized by Takara (Tokyo, Japan) (Table 2). Relative quantification method $2^{-\Delta Ct}$ was used to calculate the relative transcription level of target gene mRNA with ΔCt calculated as follows: $\Delta Ct = Ct_{\text{(target gene)}} - Ct_{\text{(internal control)}}$, $\Delta Ct = Ct_{\text{(experimental group)}} - Ct_{\text{(control group)}}$.

Western blot analysis

The total protein was extracted from cells and tissues using radio immunoprecipitation assay (RIPA) lysis buffer containing phenylmethanesulfonyl fluoride (R0010, Beijing Solarbio Science & Technology Co., Ltd., Beijing, China). A bicinchoninic acid assay kit (Invitrogen Life Technologies, Carlsbad, CA, USA) was used to determine protein concentration. Next, the proteins were separated using 10% sodium dodecyl sulfate polyacrylamide gel electrophoresis (Beyotime Biotechnology, Shanghai, China), transferred onto a nitrocellulose membrane (Invitrogen Life Technologies, Carlsbad, CA, USA) and blocked with 5% skim milk powder overnight at 4°C. Subsequently, the membrane underwent incubation with primary rabbit antibodies against Robo1 (ab7279, 1:1000, Abcam, Cambridge, MA, USA), p-AKT (Ser473, # 4060, 1:1000, Cell Signaling, Danvers, MA, USA), AKT (#4691, 1:1000, Cell Signaling, Danvers, MA, USA), p-mTOR (ser2448, #5536, 1:1000, Cell Signaling, Danvers, MA, USA), mTOR (# 2983, 1:1000, Cell Signaling, Danvers, MA, USA), p-PI3K (abs130868, 1:1000, Absin Bioscience, Inc. Shanghai, China), PI3K (abs119725, 1:1000, Absin Bioscience, Inc. Shanghai, China), and GAPDH (ab8245, 1:1000, Abcam, Cambridge, MA, USA) at 4°C overnight. Enhanced chemiluminescence (ECL) solution (1 ml) was prepared according to the instructions of SuperSignal® West Dura Extended Duration Substrate, followed by incubation at room temperature and transferring onto the membrane. After 1 min the ECL solution was removed and the membrane was sealed with fresh-keeping film

Table 1. Association between miR-29a-3p/Robo1 expression and clinicopathological characteristics of HCC patients ($n = 90$).

Clinical feature	Number ($n = 90$)	miR-29a-3p expression		p value	Robo1 expression		p value
		High	Low		High	Low	
		($n = 45$)	($n = 45$)		($n = 45$)	($n = 45$)	
Gender				0.069			0.069
Male	77	42 (54.54%)	35 (45.45%)		35 (45.45%)	42 (54.54%)	
Female	13	3 (23.08%)	10 (76.92%)		10 (76.92%)	3 (23.08%)	
Age				0.131			0.132
>50 years	36	22 (61.11%)	14 (38.89%)		14 (38.89%)	22 (61.11%)	
⩽50 year	54	23 (42.59%)	31 (57.41%)		31 (57.41%)	23 (42.59%)	
HBsAg				0.014			0.014
positive	77	43 (55.84%)	34 (44.16%)		34 (44.16%)	43 (55.84%)	
negative	13	2 (15.38%)	11 (84.62%)		11 (84.62%)	2 (15.38%)	
Cirrhosis				0.397			0.089
yes	49	22 (44.90%)	27 (55.10%)		29 (59.18%)	20 (40.82%)	
no	41	23 (56.10%)	18 (43.90%)		16 (39.02%)	25 (60.98%)	
AFP				0.82			0.495
⩾20 ng/ml	62	30 (48.39%)	32 (51.61%)		29 (46.77%)	33 (53.23%)	
<20 ng/ml	28	15 (53.57%)	13 (46.43%)		16 (57.14%)	12 (42.86%)	
Tumor size				0.202			>0.999
>5 cm	51	22 (43.14%)	29 (56.86%)		26 (50.98%)	25 (49.02%)	
⩽5 cm	39	23 (58.97%)	16 (41.03%)		19 (48.72%)	20 (51.28%)	
Tumor number				0.495			0.495
multiple	28	12 (42.86%)	16 (57.14%)		12 (42.86%)	16 (57.14%)	
single	62	33 (53.23%)	29 (46.77%)		33 (53.23%)	29 (46.77%)	
Tumor thrombus				0.028			0.08
yes	33	22 (66.67%)	11 (33.33%)		12 (36.36%)	21 (63.64%)	
no	57	23 (40.35%)	34 (59.65%)		33 (57.89%)	24 (42.11%)	
Edmondson–Steiner				0.003			0.001
I–II	45	30 (66.67%)	15 (33.33%)		14 (31.11%)	31 (68.89%)	
III–IV	45	15 (33.33%)	30 (66.67%)		31 (68.69%)	14 (31.11%)	
TNM stage				0.005			0.001
I–II	40	13 (32.50%)	27 (67.50%)		28 (70.00%)	12 (30.00%)	
III–IV	50	32 (64.00%)	18 (36.00%)		17 (34.00%)	33 (66.00%)	

Chi-square test was applied to access the association between miR-29a-3p/Robo1 expression and the clinicopathological characteristics.
AFP, alpha fetoprotein; HBsAg, hepatitis B surface antigen; HCC, hepatocellular carcinoma; miR-29a-3p, microRNA-291-3p; Robo1, roundabout homolog 1; TNM, tumor lymph node metastasis.

and placed in a dark box for 5–10 min of X-ray film exposure for development. The immunocomplexes on the membrane were visualized using luminometer (GE, USA), band intensities were quantified using the Image Pro Plus 6.0 (Media Cybernetics, USA). The ratio of the gray value of the target band to GAPDH was representative of the relative protein expression. The experiment was run in triplicate independently.

Immunohistochemistry

HCC and paracancerous tissues, normal liver and subcutaneous tumor tissues were fixed in 10% formalin solution, paraffin-embedded, and sliced into sections. After being dewaxed, the sections were hydrated and blocked with endogenous peroxidase followed by microwave treatment with 10 mmol/L sodium citrate buffer for 20 min. Next, incubation was carried out on the sections with the primary antibody against Robo1 (ab7279, 1:100) and Ki-67 (ab16667, 1:1000) overnight at 4°C. After being rinsed three times with phosphate buffer saline (PBS), the sections were incubated with secondary horseradish peroxidase-labeled goat anti-rabbit immunoglobulin G (IgG; 1: 1000, ab6721). All antibodies were purchased from Abcam (Cambridge, MA, USA). The primary antibody was replaced with PBS as a NC. Five high-power fields were randomly selected and observed under an optical microscope (CX41-12C02, Olympus, Tokyo, Japan); the cells which appeared to have brown-yellow particles were considered positive. Afterwards, four representative images were captured using a 200× optical microscope (CX41-12C02, Olympus, Tokyo, Japan) under the same setting model. Robo1 positive cells were counted. The glass slides were set at the uniform model to record the staining of each antibody. Robo1 positively stained integral optical density (IOD) was measured in each image, and the ratio of IOD to the total area of each image was regarded as the density of Robo1.[20]

Immunofluorescence staining

After 48-h transfection, the cell slide was washed three times with PBS (5 min each time), fixed with 4% of paraformaldehyde at room temperature for 30 min, and treated with 0.2% of Triton X-100 at room temperature for 15 min, after which it was blocked with 3% bovine serum albumin at 4°C for 30 min. Next, the cell slide was incubated first with primary antibodies against Robo1 (1:50, ab7279) and alpha fetoprotein (AFP) (1:100, ab169552), then with fluorescent secondary antibodies (ab150077, 1:200; ab150115, 1:200) avoiding light exposure at room temperature for 2 h. All the antibodies were purchased from Abcam (Cambridge, MA, USA). Afterwards, 4',6-diamidino-2-phenylindole (ab104139, 1:100, Abcam, Cambridge, MA, USA) was added to the cell slide for 10-min staining at room temperature devoid of light exposure. The slide was then washed 3 times with PBS (5 min/time) and sealed with mounting medium, after which it was observed under an inverted fluorescence microscope.

Table 2. Primer sequences for RT-qPCR.

Gene	Primer sequence
miR-29a-3p	F: 5'-GGGTAGCACCATCTGAAAT-3'
	R: 5'-CAGTGCGTGTCGTGGAGT-3'
LINC00473	F: 5'-GGCAGCCTCAGGTTACAAAT-3'
	R: 5'-AGGAGCAGGTAGGGAAATGA-3'
Robo1	F: 5'-AAAGTAGCACGACGGCAAAT-3'
	R: 5'-GGCACTGAGACGCATGAAA-3'
U6	F: 5'-CTCGCTTCGGCAGCACA-3'
	R: 5'-AACGCTTCACGAATTTGCGT-3'
GAPDH	F: 5'-AGCCACATCGCTCAGACAC-3'
	R: 5'-GCCCAATACGACCAAATCC-3'

F, forward; GAPDH, glyceraldehyde-3-phosphate dehydrogenase; LINC00473, long non-coding RNA LINC00473; miR-29a-3p, microRNA-29a-3p; R, reverse; Robo1, roundabout homolog 1; RT-qPCR, reverse transcription quantitative polymerase chain reaction.

Dual-luciferase reporter gene assay

Target binding site of miR-29a-3p and Robo1 was predicted using the TargetScan database (www.targetscan.org). The synthetic wild type (WT) and mutant (MUT) 3' untranslated region (3'-UTR) of Robo1 genes were inserted into the luciferase reporter vector pGL3-control vector (Promega, Madison, WI, USA). The correctly sequenced luciferase reporter plasmids WT and MUT were then co-transfected with miR-29a-3p mimic, mimic NC, miR-29a-3p inhibitor, or inhibitor NC into 293T cells. Following 48-h transfection, the cells were collected and lysed. Subsequently, the luciferase activity was measured using a luciferase assay kit (K801-200, Biovision, San Francisco, USA) and a Glomax

20/20 luminometer fluorescence detector (Promega, Madison, Wisconsin, USA). The target relationship between LINC00473 and miR-29a-3p was detected using the same method mentioned in the previous. The experiment was conducted in triplicate.

Cell counting kit-8 (CCK-8) assay

The cells were seeded in a 96-well plate at a density of 2×10^3 cells/well (approximately 100 µl cell suspension/well), involved at least 3 wells, each repeated in triplicate, which was considered as the starting point (0 h). Then the cells were added with 100 µl CCK-8 in order to assess cell activity at the wavelength of 450 nm at 0, 24, 48, and 72 h according to the CCK-8 kit (Beyotime Biotechnology, Wuhan, Hubei, China).[21]

Colony formation assay

After transfection, 200 cells were counted and plated onto 12-well plates. Fresh culture medium was replaced every 3 days, and colonies were counted 14 days after plating. The cells were then stained with crystal violet. The number of colonies containing more than 50 cells was assessed under a microscope, as previously described. All experiments were performed in triplicate.[22]

Transwell assay

Transwell chambers (Boyden chambers; Corning, Cambridge, MA, USA) were used to detect cell invasion and migration. The cells were suspended in serum-free medium at a density of 5×10^5 cells/ml. A total of 200 µl cell suspension was added to the apical chamber of Transwell chambers to detect cell migration. Next, 200 µl cell suspension was added to the Transwell apical chamber coated with Matrigel (Corning, Cambridge, MA, USA) to measure cell invasion. Next, 600 µl DMEM containing 10% FBS was added to the Transwell basolateral chamber. After 24-h incubation, the cells in the apical chamber were wiped off with a cotton swab, and the remaining cells were fixed with formaldehyde, and stained using crystal violet (Sigma Aldrich, San Francisco, CA, USA) for 10 min. Finally, the cells were observed in five randomly selected visual fields under an inverted microscope (CX22; Olympus, Tokyo, Japan). The experiment was conducted in triplicate.

Xenograft tumor in nude mice

BALB/c nude mice (aged 4–6 weeks; weighing 16–20 g) (Hunan SJA Laboratory Animal Co., Ltd., Hunan, China) were raised at constant temperature of 25–27°C and humidity of 45–50%. Next, 2×10^6 Huh7-Luc-labeled cells (Genechem, Shanghai, China) were re-suspended in 200 µl normal saline, after which they were subcutaneously injected into the left or right forelimb of each nude mouse. When the tumor volume exceeded 100 mm^3 in all nude mice, the nude mice were randomly classified into 6 groups with 15 mice placed in each group: (a) blank group, (b) LV-miR-29a-3p group, (c) LV-NC group, (d) LV-sh Robo1 group, (e) LV-shCon group, (f) LV-miR-29a-3p + LV-sh Robo1 group. The mice in the blank group were injected with normal saline, while the mice in the remaining groups were injected with the corresponding lentiviruses (5 nmol/mouse, 3 days/time) for 14 days. The tumor length (L) and width (W) of the mice were measured by Vernier calipers every 3 days. The tumor volume was calculated using the following formula: $V = L \times W^2 \times 0.5$. The growth curve was drawn. All nude mice were euthanized 15 days after inoculation, and the tumors were excised and weighed. Tumor tissues were obtained for immunohistochemistry and immunofluorescence.

Subsequently, the previously mentioned tumor tissues that had been injected with Huh7-Luc-labeled cells were cut into 1 mm^2 of pieces and implanted into the left lobe of each BALB/c male nude mouse. The nude mice were grouped using the same method mentioned previously, and then transduced with corresponding lentiviruses *via* tail vein injection (20 nmol/mouse, 3 days/time) for 15 days. The *in vivo* imaging of mice was performed using the Xenogen IVIS system on the 9th day and the 15th day to observe the growth, invasion, metastasis, and survival of the tumor.

RNA-binding protein immunoprecipitation

RIP kit (Millipore, Stafford, VA, USA) was used for detection. The HCCLM3 cells were washed with pre-cooled PBS, after which the supernatant was removed. The cells were then lysed with an equal volume of RIPA lysis buffer (Sigma Aldrich, SF, CA, USA) for 5 min in an ice bath, and the supernatant was obtained. Next, the cells were incubated with 5 µg rabbit antibody against Ago2 (ab32381, 1:50, Abcam, Cambridge, MA, USA) for combination. The magnetic bead–antibody

complex was re-suspended in 900 µl RIP wash buffer and incubated with 100 µl cell extract at 4°C overnight. IgG (Millipore, Stafford, VA, USA) served as a NC and SNRNP70 (Millipore, Stafford, VA, USA) was considered as the positive control. RNA was extracted for subsequent PCR detection.

RNA-pull down assay

HCCLM3 cells were transfected with Biotinylated miR-129-5p-Bio, miR-129-5p-Bio-MUT and corresponding NC-Bio.[23] After 48 h of transfection, the cells were lysed with lysis buffer and incubation was carried out with streptavidin magnetic beads (Life Technologies, Carlsbad, CA, USA) at 4°C for 4 h. Next, RNA was extracted using Trizol, and RT-qPCR was carried out to detect the expression of lncRNA LINC00473.

Statistical analysis

All data were processed using SPSS 21.0 statistical software (IBM Corp. Armonk, NY, USA). The measurement data were expressed as mean ± standard deviation. All data were tested for normal distribution and homogeneity of variances. If no deviations were observed, the paired *t*-test was used for intragroup comparison, while unpaired *t*-test was used for comparison between groups, and one-way analysis of variance (ANOVA) or repeated measures ANOVA was performed for comparison among multiple groups. Otherwise, the rank test was carried out. $p < 0.05$ was considered a statistically significant difference.

Results

HCC tissues and cells exhibit elevated expression of Robo1

RT-qPCR and Western blot analysis were conducted in order to examine the expression of Robo1 in HCC, paracancerous, and normal liver tissues to determine its role in the development of HCC. The results showed that there was a higher expression of Robo1 in HCC tissues compared with the paracancerous and normal liver tissues (Figure 1A–C). As determined by immunohistochemistry and immunofluorescence staining, the ratio of Robo1 positive cells was increased in HCC tissues relative to paracancerous and normal liver tissues, which provided further evidence that Robo1 was upregulated in HCC tissues and had more stable expression than the commonly used tumor marker AFP (Figure 1D). Moreover, the expression of Robo1 was correlated with HBsAg ($p = 0.014$) and Edmondson–Steiner ($p = 0.001$) classification in HCC patients (Table 1). HCC patients with upregulated Robo1 presented with a lower survival rate (Figure 1E) but higher recurrence rate than those with downregulated Robo1 (Figure 1F). Next, the expression of Robo1 was determined in four human HCC cell lines and one immortalized human liver cell line. Based on the findings there was a higher expression of Robo1 in the four HCC cell lines *versus* the immortalized human liver cell line L02 (Figure 1G–H). These results suggested that the up-regulation of Robo1 might be associated with HCC tumorigenesis.

Silencing of Robo1 suppresses cell proliferation, migration, and invasion in HCC

After Robo1 was knocked down in HCCLM3 and HepG2 cells, the Robo1 expression was decreased. LV-sh-Robo1#1 was then selected for subsequent experiments (Figure 2A). The results from CCK-8 (Figure 2B) revealed that cell proliferation was inhibited following the knockdown of Robo1, which was further demonstrated in colony formation assay (Figure 2C). Transwell assay was performed to evaluate the effects of the knockdown of Robo1 on HCC cell migration and invasion. It was shown that Robo1 silencing could result in the inhibition of HCC cell migration and invasion (Figure 2D). A previous study revealed that Robo1 affects tumor growth in breast cancer through the PI3K/AKT signaling pathway.[24] Consistently, our findings also demonstrated that knockdown of Robo1 led to the inactivation of the PI3K/AKT/mTOR signaling pathway (Figure 2E). The previously mentioned findings suggested that HCC cell proliferation, migration, and invasion were suppressed as a result of Robo1 silencing.

miR-29a-3p targets and negatively regulates Robo1

The regulatory effect of miRNA on Robo1 was predicted using 5 databases including DIANA to broaden our understanding on the effect of Robo1 on HCC, and the results found an intersection between the 5 databases (Figure 3A). Finally, five potential regulatory miRNAs of Robo1 gene were found. Further quantitative analysis on these 5 miRNAs revealed that miR-29a-3p had the most significant differential expression in HCC.

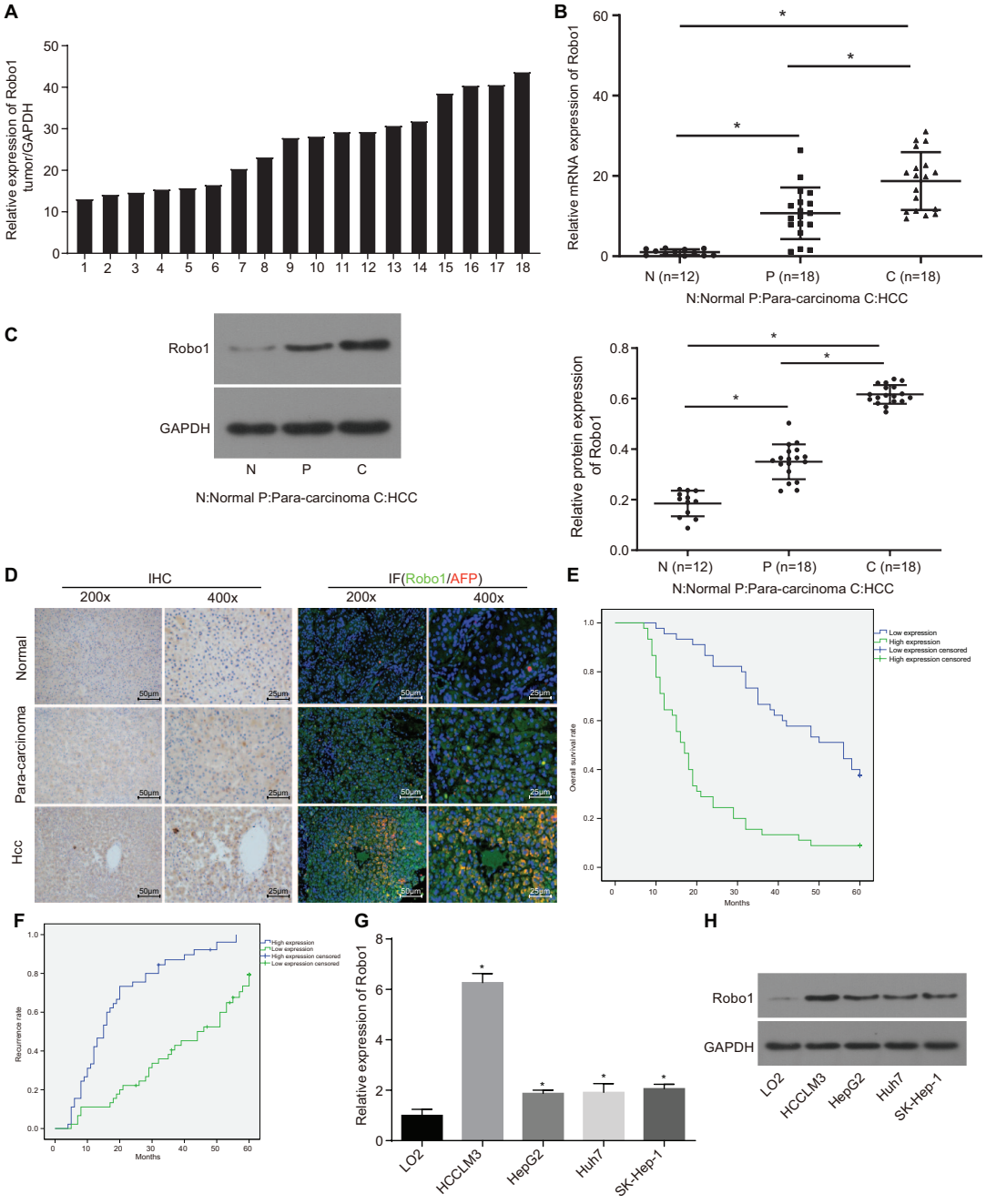

Figure 1. Robo1 was highly expressed in HCC tissues and cells. (A) the expression of Robo1 in 18 cases of HCC tissue samples determined by RT-qPCR, normalized to GAPDH; the number in the graph represented the sample number; (B) the expression of Robo1 in 18 cases of HCC tissues, 18 cases of paracancerous tissues and 12 cases of normal liver tissues examined by RT-qPCR; (C) the protein expression of Robo1 in HCC, paracancerous and normal liver tissues detected by Western blot analysis. The value of each sample point in the statistical graph = gray value of Robo1 protein band in samples/gray value of GAPDH protein band in samples/normalization value. ($^{*}p < 0.05$, $^{**}p < 0.01$, $^{***}p < 0.001$); (D) the expression of Robo1 in HCC tissues examined by immunohistochemistry, and immunofluorescence staining (left, 200×; right, 400×); (E) the correlation between survival rate of HCC patients and expression of Robo1 analyzed by Kaplan–Meier method; (F) the correlation between recurrence rate of HCC patients and expression of Robo1 analyzed by Kaplan–Meier method; (G) the expression of Robo1 in HCC and normal liver cell lines; (H) the expression of Robo1 in HCC and normal liver cell lines determined by Western blot analysis; $n = 3$. Data were analyzed using one-way analysis of variance.

GAPDH, glyceraldehyde-3-phosphate dehydrogenase; HCC, hepatocellular carcinoma; RT-qPCR, reverse transcription quantitative polymerase chain reaction.

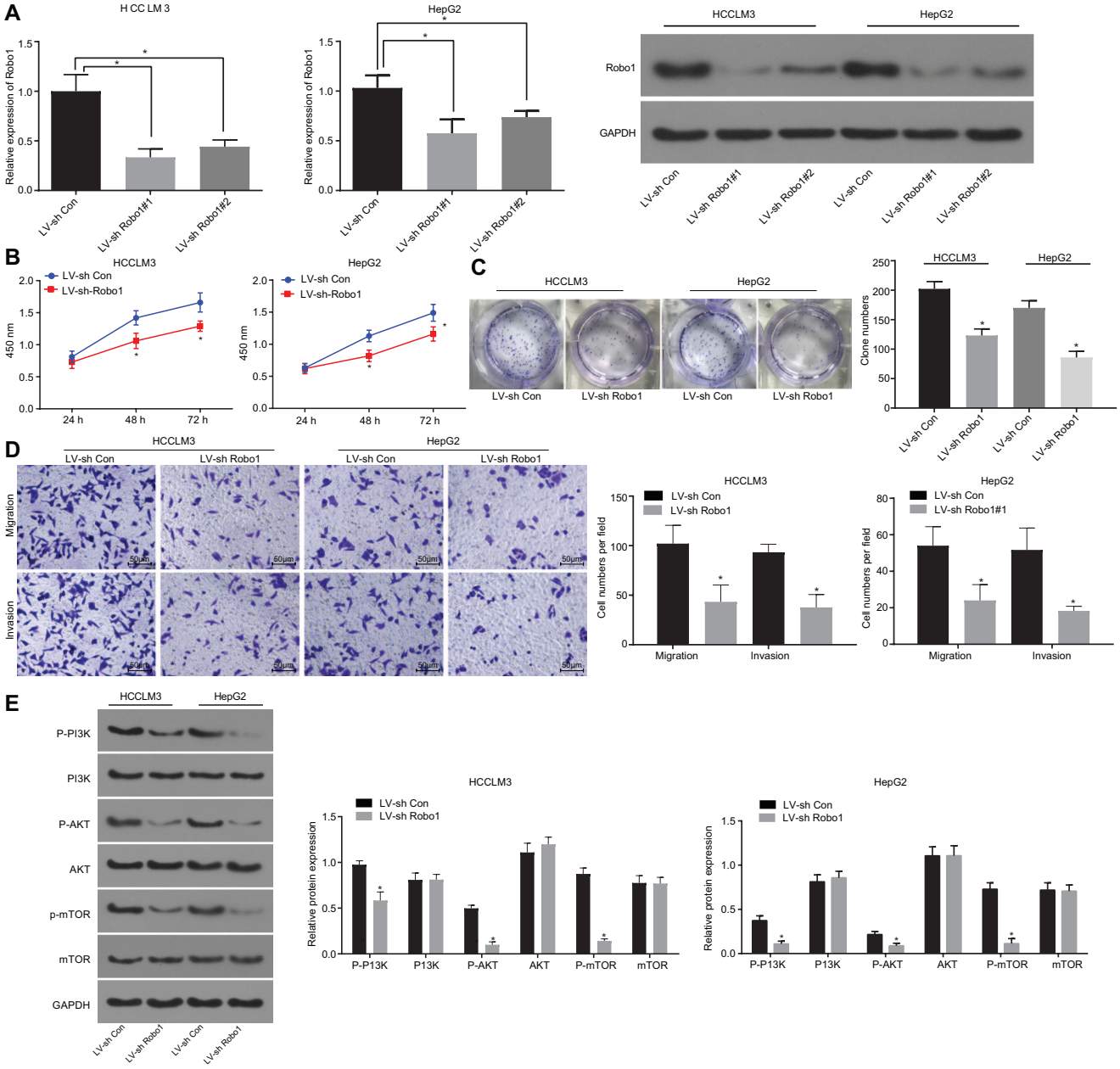

Figure 2. Knockdown of Robo1 inhibited HCC cell proliferation, migration, and invasion. (A) the expression of Robo1 in HCC cells examined by RT-qPCR and Western blot analysis; (B) HCC cell proliferation determined by CCK-8; (C) the number of clones of HCC cells examined by colony formation assay; (D) HCC cell migration and invasion examined by Transwell assay (200×); (E) Western blot analysis of the PI3K/AKT/mTOR signaling pathway-related proteins in cells; $^{*}p < 0.05$, compared with the LV-shCon group, $n = 3$. Data in panel B were analyzed by repeated measures ANOVA, data in panel D were analyzed by unpaired t test, and data in the remaining panels were analyzed by one-way ANOVA.

ANOVA, analysis of variance; HCC, hepatocellular carcinoma; LV-sh, lentivirus short hairpin; RT-qPCR, reverse transcription quantitative polymerase chain reaction.

TargetScan website predicted a binding site between miR-29a-3p and the 3'-UTR of Robo1. Dual-luciferase reporter gene assay showed that in the presence of miR-29a-3p mimic, there was a decrease in the luciferase activity of WT-Robo1 but the luciferase activity of MUT-Robo1 was not affected. However, in the presence of miR-29a-3p inhibitor, the luciferase activity of WT-Robo1 was increased while that of MUT-Robo1 showed no changes (Figure 3B). Furthermore, overexpression of miR-29a-3p resulted in a reduction in Robo1 mRNA and protein levels, and silencing of

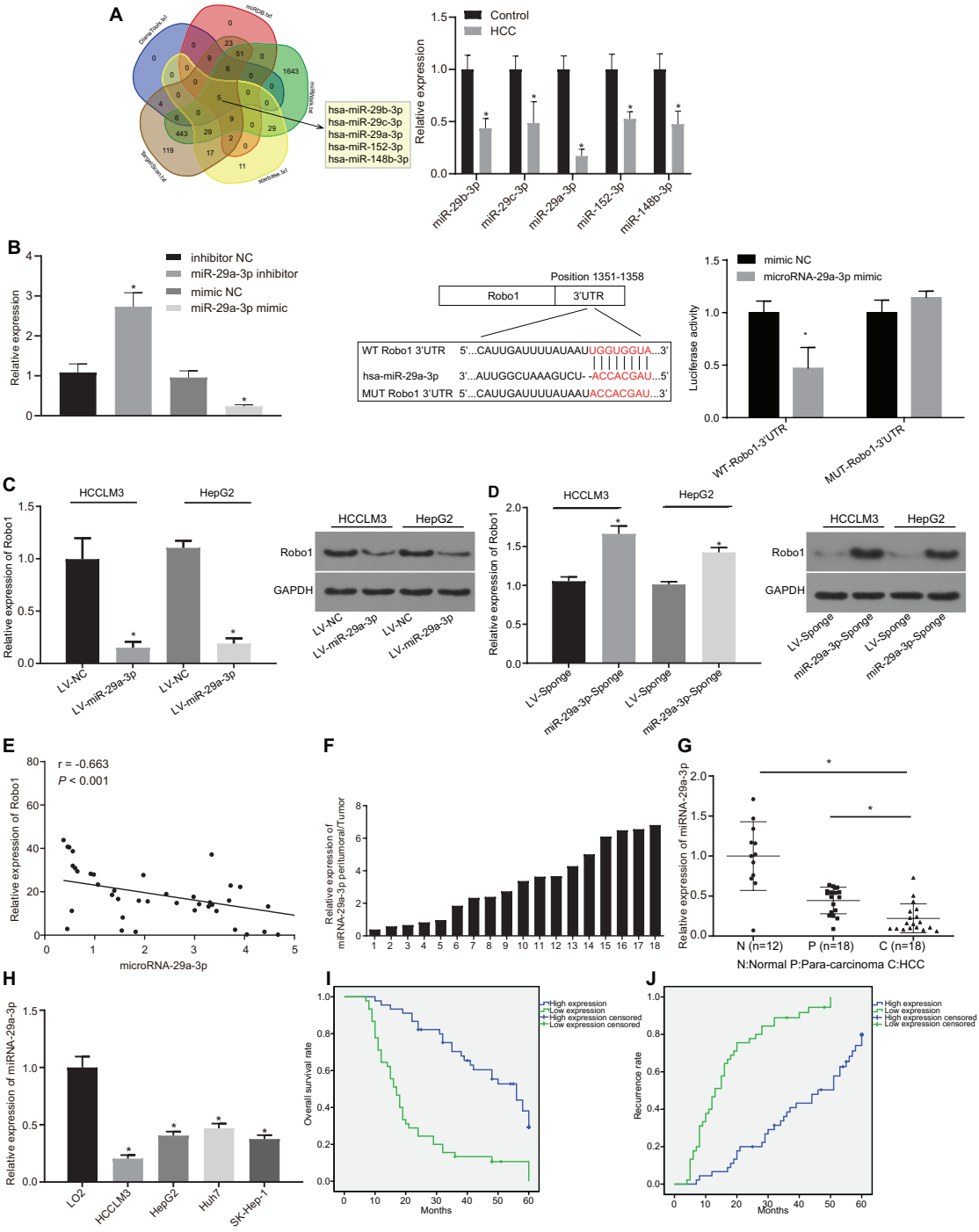

Figure 3. miR-29a-3p negatively regulated Robo1 and miR-29a-3p was poorly expressed in HCC tissues and cell lines. (A) the predicted miRNAs regulating Robo1; the five ovals in the figure represented the predicted results of miRNAs regulating Robo1 in five databases and middle part represented the intersection of the predicted results in five databases; (B) predicted binding sites between miR-29a-3p and Robo1 3'-UTR and the target relationship between miR-29a-3p and Robo1 verified by dual luciferase reporter assay; $^{*}p < 0.05$, compared with the mimic NC or inhibitor NC group, $n = 3$. t test was used for data analysis; (C–D) the expression of Robo1 in HCC cells in response to overexpressed and inhibited miR-29a-3p examined by RT-qPCR and Western blot analysis ($^{*}p < 0.05$, compared with LV-NC group or LV-Sponge group); (E) the correlation between miR-29a-3p and Robo1 expression in HCC tissues analyzed by Pearson's correlation analysis; (F) the expression of miR-29a-3p in HCC, paracancerous and normal liver tissues examined by RT-qPCR as well as the ratio of miR-29a-3p expression in paracancerous tissues to that in HCC tissues; the number in the graph represented the sample number; (G) the expression of miR-29a-3p in HCC, paracancerous and normal liver tissues determined by RT-qPCR ($^{*}p < 0.05$); (H) the expression of miR-29a-3p in HCC and normal liver cell lines determined by RT-qPCR ($^{*}p < 0.05$, compared with L02 cell lines; $n = 3$, t test was used for data analysis); (I–J) the correlation between survival rate and recurrence rate of HCC patients and miR-29a-3p expression analyzed by the Kaplan–Meier method. 3'-UTR, 3' untranslated region; HCC, hepatocellular carcinoma; LV-NC, lentivirus-negative control; miRNAs, microRNAs; RT-qPCR, reverse transcription quantitative polymerase chain reaction.

miR-29a-3p led to opposite results (Figure 3C–D). In addition, a negative correlation was observed between miR-29a-3p and Robo1 expression by Pearson's correlation analysis ($r = -0.663$, $p < 0.001$; Figure 3E). Hence, these findings indicated that miR-29a-3p might play an essential part in tumorigenesis by downregulating Robo1.

miR-29a-3p is poorly expressed in HCC tissues and cells

RT-qPCR was conducted to evaluate the expression of miR-29a-3p in HCC, paracancerous and normal liver tissues to determine its specific role in the progression of HCC. The results (Figure 3F, G) clarified that the expression of miR-29a-3p was lower in HCC tissues than that in paracancerous and normal liver tissues. HCC cell lines also presented with lower expression of miR-29a-3p (Figure 3H). Moreover, the expression of miR-29a-3p was associated with HBsAg ($p = 0.014$), tumor thrombosis ($p = 0.028$), Edmondson–Steiner classification ($p = 0.003$) and tumor node metastasis stage ($p = 0.005$) of HCC patients (Table 1). HCC patients with higher expression of miR-29a-3p presented with a higher survival rate (Figure 3I) but lower recurrence rate than those with lower expression (Figure 3J), all of which indicated that miR-29a-3p was decreased in HCC tissues and cells.

Robo1 rescues the inhibitory effect of miR-29a-3p on proliferation, migration, and invasion of HCC cells

In order to determine the regulatory effects of miR-29a-3p on HCC proliferation, migration, and invasion, miR-29-3p expression was overexpressed or inhibited (Figure 4A). It was observed that LV-miR-29a-3p promoted miR-29a-3p expression, and miR-29a-3p-sponge resulted in the suppression of its expression. From the previously mentioned assays, HCCLM3 and Huh7 cells were selected for the following experiments. CCK-8 and colony formation assay showed that the overexpression of miR-29a-3p inhibited proliferation and clone formation of HCCLM3 cells. However, the downregulation of miR-29a-3p led to an enhancement in proliferation and clone formation of Huh7 cells (Figure 4B, C). As detected by Transwell assay, miR-29a-3p upregulation could lead to the suppression of migration and invasion of HCCLM3 cells, while downregulation of miR-29a-3p induced migration and invasion of Huh7 cells (Figure 4D). Moreover, Western blot analysis suggested that miR-29a-3p elevation inactivated the PI3K/AKT/mTOR signaling pathway, whereas miR-29a-3p silencing activated the PI3K/AKT/mTOR signaling pathway (Figure 4E). In addition, the inhibitory effects of miR-29a-3p on proliferation, colony formation, migration, and invasion on HCCLM3 cells could be reversed by Robo1 (Figure 4B–D). The aforementioned findings suggested that Robo1 could rescue the inhibitory effects of miR-29a-3p on proliferation, migration, and invasion of HCC cells.

miR-29a-3p overexpression or inhibited Robo1 represses HCC cell growth and metastasis in vivo

Xenograft tumor in nude mice was performed to further verify the aforementioned results *in vivo*, and the results found that elevated miR-29a-3p expression or inhibited Robo1 resulted in the suppression of tumor volume and growth *in vivo* (Figure 5A–C). As determined by immunohistochemistry, the level of Ki-67 and HCC cell proliferation were repressed in response to the miR-29a-3p upregulation or Robo1 downregulation *in vivo* (Figure 5D). The results of immunohistochemistry and immunofluorescence suggested that there was a decrease in Robo1, and its expression could be inhibited by miR-29a-3p following the knockdown of Robo1 (Figure 5E). *In vivo* fluorescence imaging further confirmed that miR-29a-3p overexpression or Robo1 knockdown attenuated tumor growth and metastasis to the spleen, lung, kidney, and intestine on day 15 (Figure 5F). Survival analysis revealed that the elevation of miR-29a-3p or silencing of Robo1 promoted survival of nude mice (Figure 5G). The aforementioned results provided evidence that miR-29a-3p overexpression or Robo1 silencing resulted in the inhibition of HCC cell growth and metastasis *in vivo*.

LINC00473 competitively binds to miR-29a-3p to upregulate Robo1 expression

A previous study that was conducted to identify the subcellular location of LINC00473 in cells revealed that LINC00473 was expressed in both nucleus and cytoplasm.[25] In recent years, the interaction pattern of ceRNA has been widely reported. Therefore, in order to determine whether LINC00473 served as a ceRNA in HCC, the binding site between LINC00473 and miR-29a-3p was predicted using bioinformatics (http://

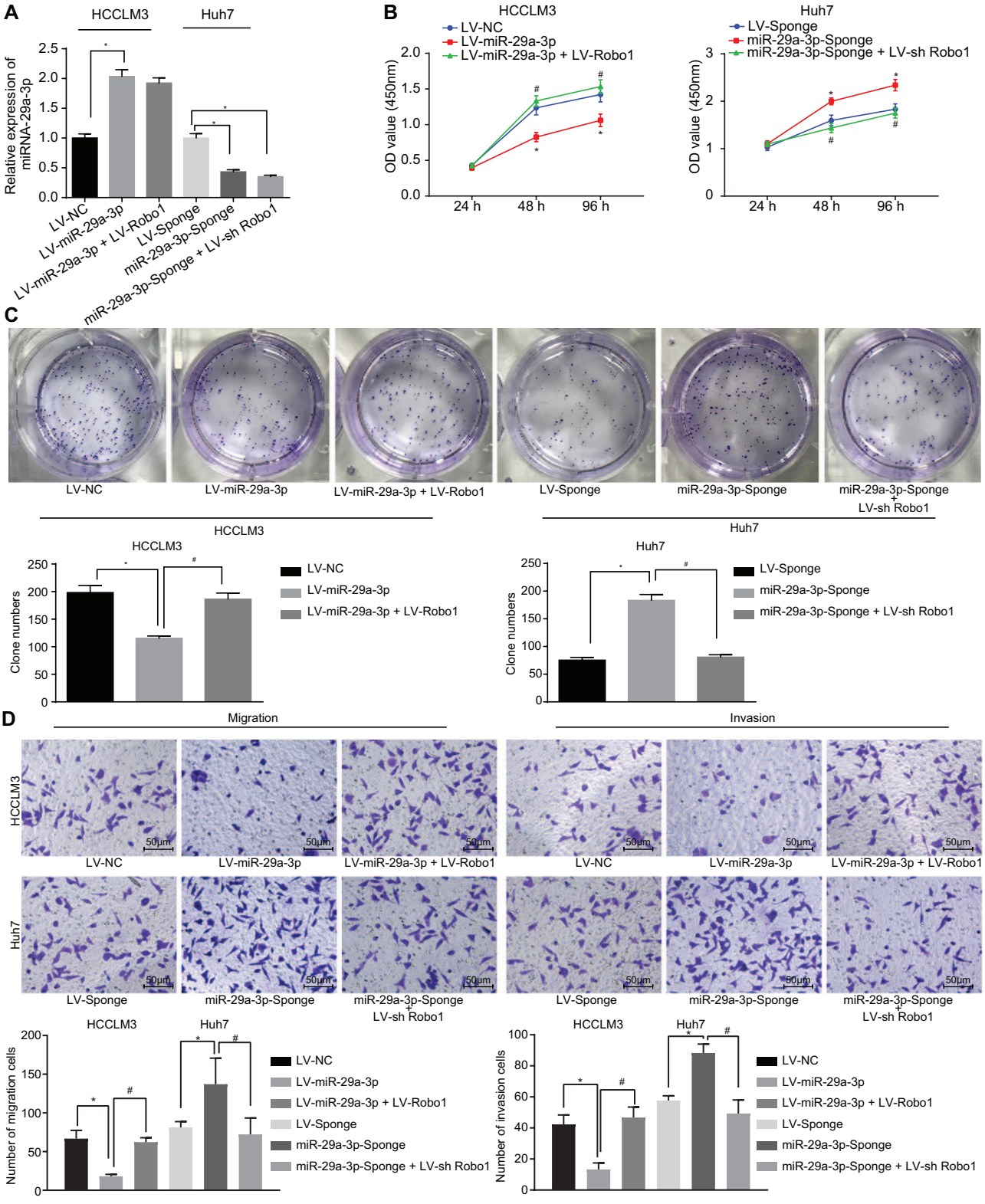
A
HCCLM3
Huh7
Relative expression of miRNA-29a-3p
LV-NC
LV-miR-29a-3p
LV-miR-29a-3p + LV-Robo1
LV-Sponge
miR-29a-3p-Sponge
miR-29a-3p-Sponge + LV-sh Robo1
B
HCCLM3
LV-NC
LV-miR-29a-3p
LV-miR-29a-3p + LV-Robo1
OD value (450nm)
24 h
48 h
96 h
Huh7
LV-Sponge
miR-29a-3p-Sponge
miR-29a-3p-Sponge + LV-sh Robo1
C
LV-NC
LV-miR-29a-3p
LV-miR-29a-3p + LV-Robo1
LV-Sponge
miR-29a-3p-Sponge
miR-29a-3p-Sponge + LV-sh Robo1
HCCLM3
Huh7
Clone numbers
D
Migration
Invasion
HCCLM3
Huh7
50μm
Number of migration cells
Number of invasion cells

(Continued)

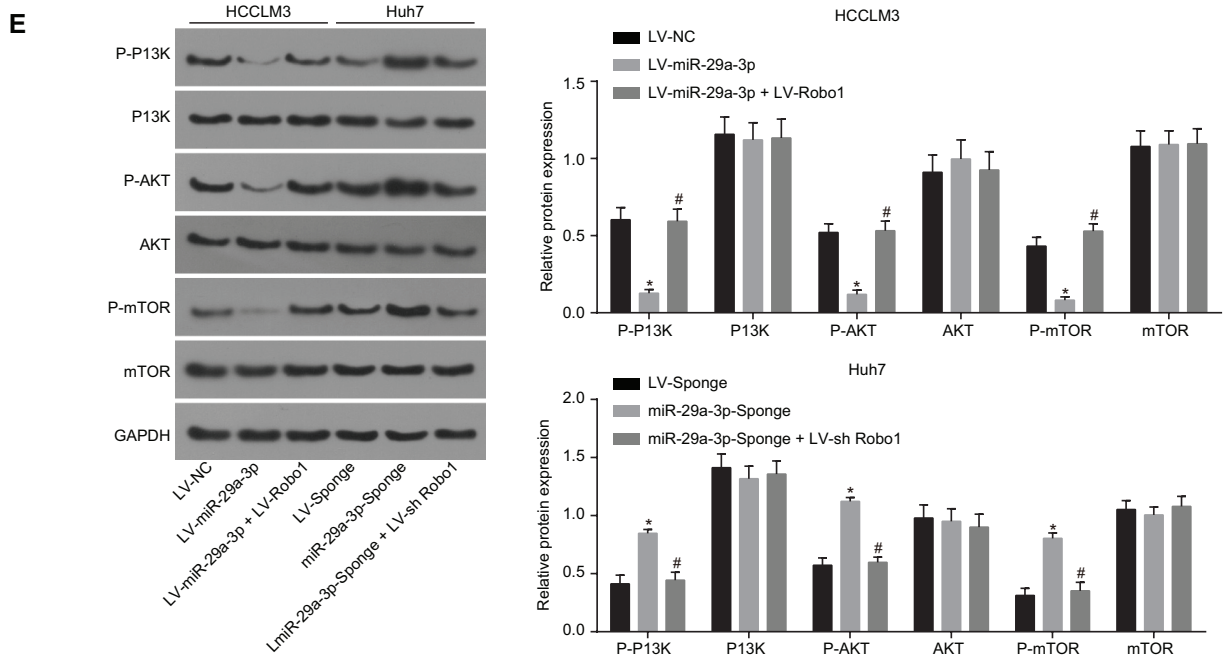

Figure 4. Robo1 reversed the inhibitory role of miR-29a-3p in proliferation, migration, and invasion of HCC cells. (A) the expression of miR-29a-3p in HCC cells examined by RT-qPCR; (B) the proliferation of HCC cells examined by CCK-8 assay; (C) the number of clones of HCC cells examined by colony formation assay; (D) the migration and invasion of HCC cells determined by Transwell assay (200×); (E) Western blot analysis of the PI3K/AKT/mTOR signaling pathway-related proteins in cells; $^{*}p < 0.05$, compared with the LV-Sponge group or the LV-NC group; $^{\#}p < 0.05$, compared with the LV-miR-29a-3p or miR-29a-3p-Sponge groups; Data in panel B were analyzed by repeated measures ANOVA, and data in the remaining panels were analyzed by one-way ANOVA.
ANOVA, analysis of variance; HCC, hepatocellular carcinoma; LV-NC, lentivirus-negative control; RT-qPCR, reverse transcription quantitative polymerase chain reaction.

www.microrna.org) (Figure 6A), which was then validated by a series of experiments including RNA immunoprecipitation, RNA-pull down, and dual-luciferase reporter gene assay. The results of RNA immunoprecipitation showed a significant increase in LINC00473 enrichment (Figure 6B). The results from RNA pull down revealed that miR-29a-3p could pull down more LINC00473 (Figure 6C). Dual-luciferase reporter gene assay revealed an obvious decrease in luciferase activity when miR-29a-3p was co-transfected with LINC00473-WT (Figure 6D). These results demonstrated the interaction between miR-29a-3p and LINC00473. Subsequently, the role of LINC00473 was further investigated by detecting its expression in HCC-LM3 cell lines, and the results showed that LINC00473 expression was upregulated in the HCC-LM3 cell lines (Figure 6E, F). This finding suggests that LINC00473 is reversely associated with the level of miR-29a-3p in HCC. To verify this hypothesis, RT-qPCR was conducted to detect changes in miR-29a-3p expression after silencing of LINC00473, which revealed that miR-29a-3p expression was increased following LINC00473 silencing, which was similar to the findings from the correlation analysis (Figure 6C, D). Moreover, correlation analysis identified a positive interaction between LINC00473 and Robo1 (Figure 6I). In summary, LINC00473 could competitively bind to miR-29a-3p to upregulate the expression of Robo1.

Knockout of LINC00473 inhibits the proliferation, migration, and invasion of HCC cells

We next intended to further verify the role of LINC00473 in HCC cells. First, we infected HCCLM3 and HepG2 cells with lentivirus expressing sh-LINC00473, and then conducted CCK-8, colony formation, and Transwell assays. The results showed significantly reduced expression of LINC00473 in HCC cells treated with sh-LINC00473#1, sh-LINC00473#2 and sh-LINC00473#3, among which sh-LINC00473#2 showed the lowest LINC00473 expression (Figure 7A) and therefore used for subsequent experiments. As depicted in Figure 7B–D,

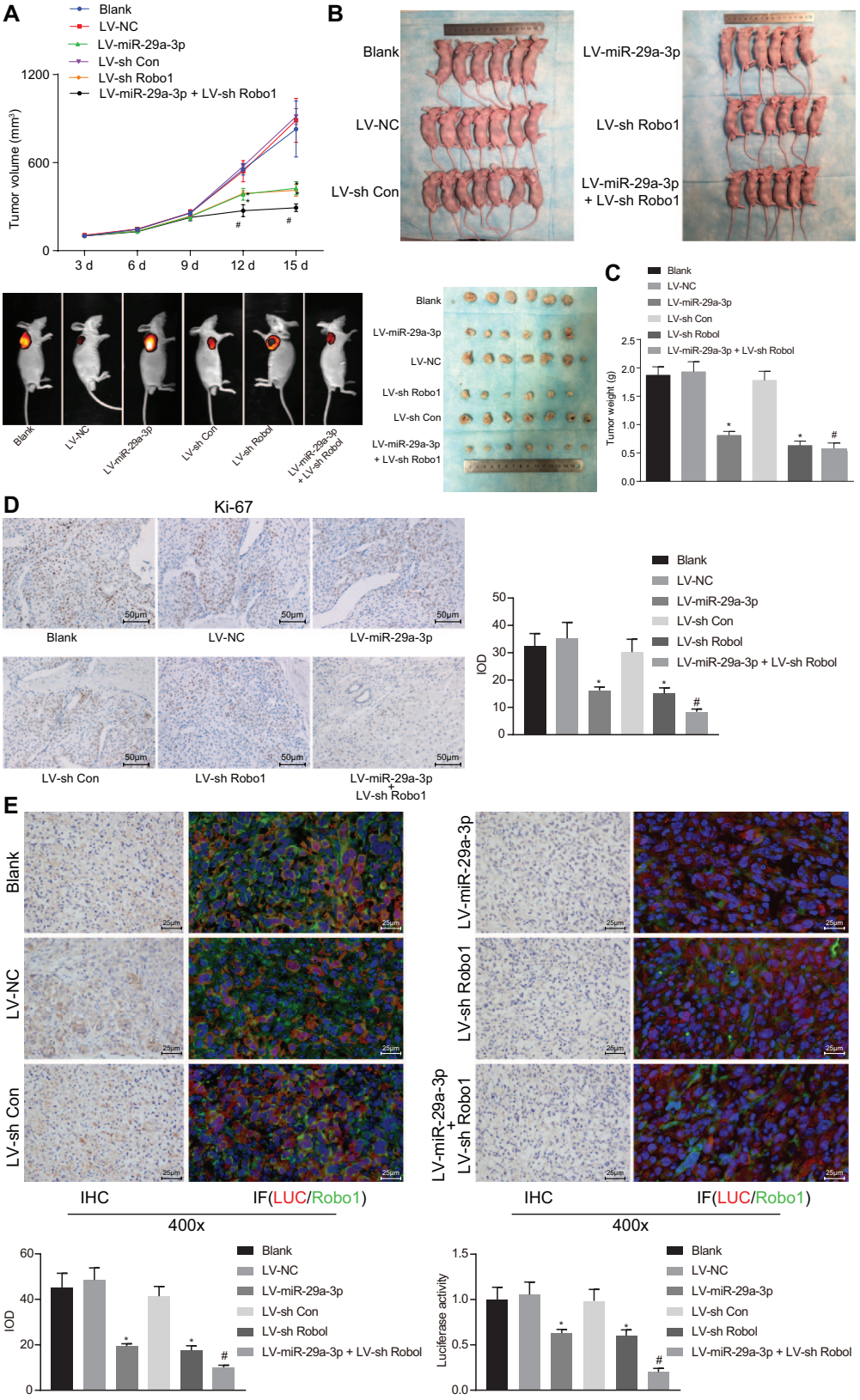
A
Blank
LV-NC
LV-miR-29a-3p
LV-sh Con
LV-sh Robo1
LV-miR-29a-3p + LV-sh Robo1
Tumor volume (mm³)
1200
600
0
3 d
6 d
9 d
12 d
15 d
B
Blank
LV-NC
LV-sh Con
LV-miR-29a-3p
LV-sh Robo1
LV-miR-29a-3p + LV-sh Robo1
C
Tumor weight (g)
D
Ki-67
IOD
E
IHC
IF(LUC/Robo1)
400x
Luciferase activity

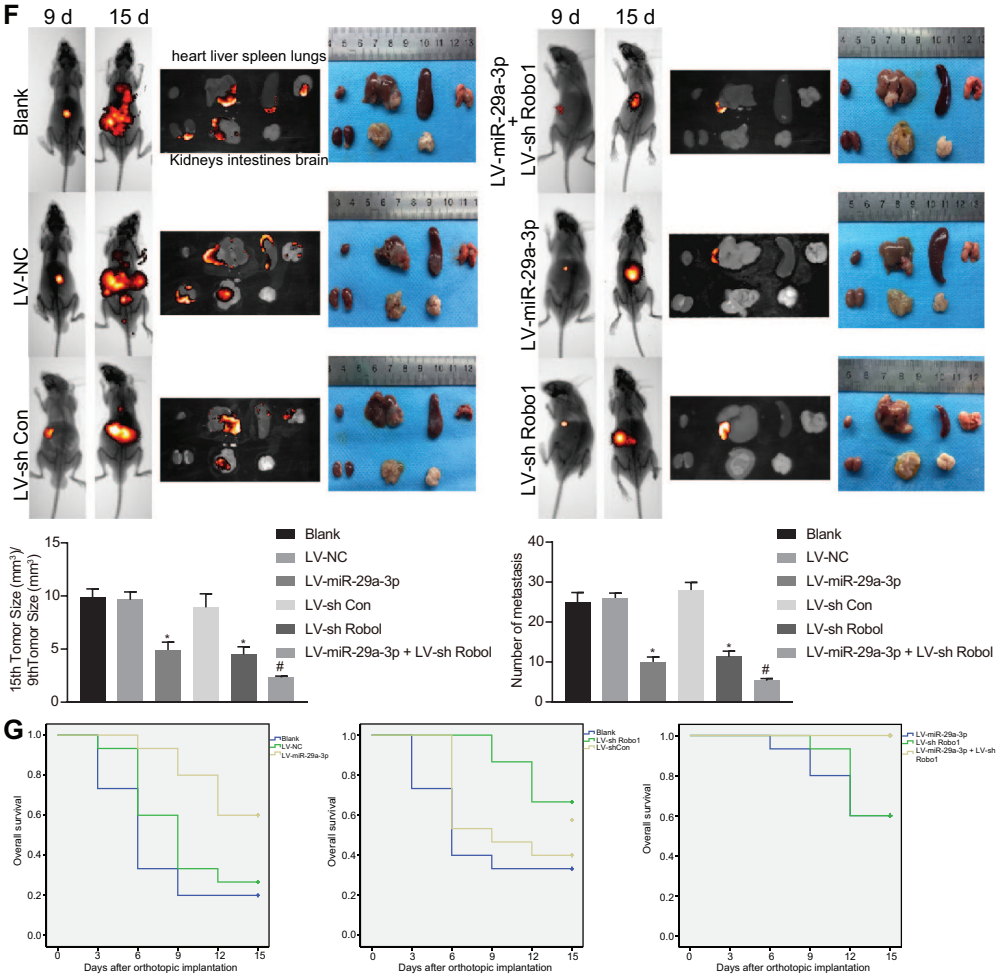

Figure 5. miR-29a-3p overexpression inhibited tumor growth and metastasis in nude mice with HCC. (A) quantitative analysis of tumor volume measured with a Vernier caliper ($^{*}p < 0.05$, compared with the LV-NC group or the LV-shCon group; $^{\#}p < 0.05$, compared with the LV-miR-29a-3p group); (B) tumor size observed by naked eyes and fluorescence imaging; (C) quantitative analysis of tumor weight of nude mice ($^{*}p < 0.05$, compared with the LV-NC group or the LV-shCon group; $^{\#}p < 0.05$, compared with the LV-miR-29a-3p group), $n = 6$; (D) the expression of Ki-67 in HCC tissues examined by immunohistochemistry (200×) and quantitative analysis; (E) the expression of Robo1 in HCC tissues determined by immunohistochemistry and immunofluorescence (400×) and quantitative analysis; (F) tumor metastasis in nude mice *in vivo* examined by fluorescence imaging and quantitative analysis; (G) the correlation of survival rate of nude mice with expression of miR-29a-3p and Robo1 analyzed by Kaplan–Meier method.
HCC, hepatocellular carcinoma; LV-NC, lentivirus-negative control; LV-sh, LV short hairpin.

silencing of LINC00473 resulted in an obvious decline in cell proliferation, migration, and invasion. Therefore, silencing of LINC00473 could impede the proliferation, migration, and invasion of HCC cells.

Discussion

Although the natural history and pathologic characteristics of human HCC are well documented, the molecular pathogenesis of HCC remains poorly understood.[26] Thus, it is of significant importance to clarify more specific biomarkers for the early detection, prevention, and treatment of HCC.[27] There is a correlation between the dysregulation of miRNAs and the pathogenesis and progression of HCC, which are widely highlighted as underlying biomarkers for HCC.[28] In addition, lncRNAs are also identified as novel biomarkers for the early detection, diagnosis and treatment of HCC.[6] Therefore, on the basis of pre-existing data, we conducted the present study to investigate the potential mechanisms of LINC00473 and miR-29a-3p in the development of HCC. In

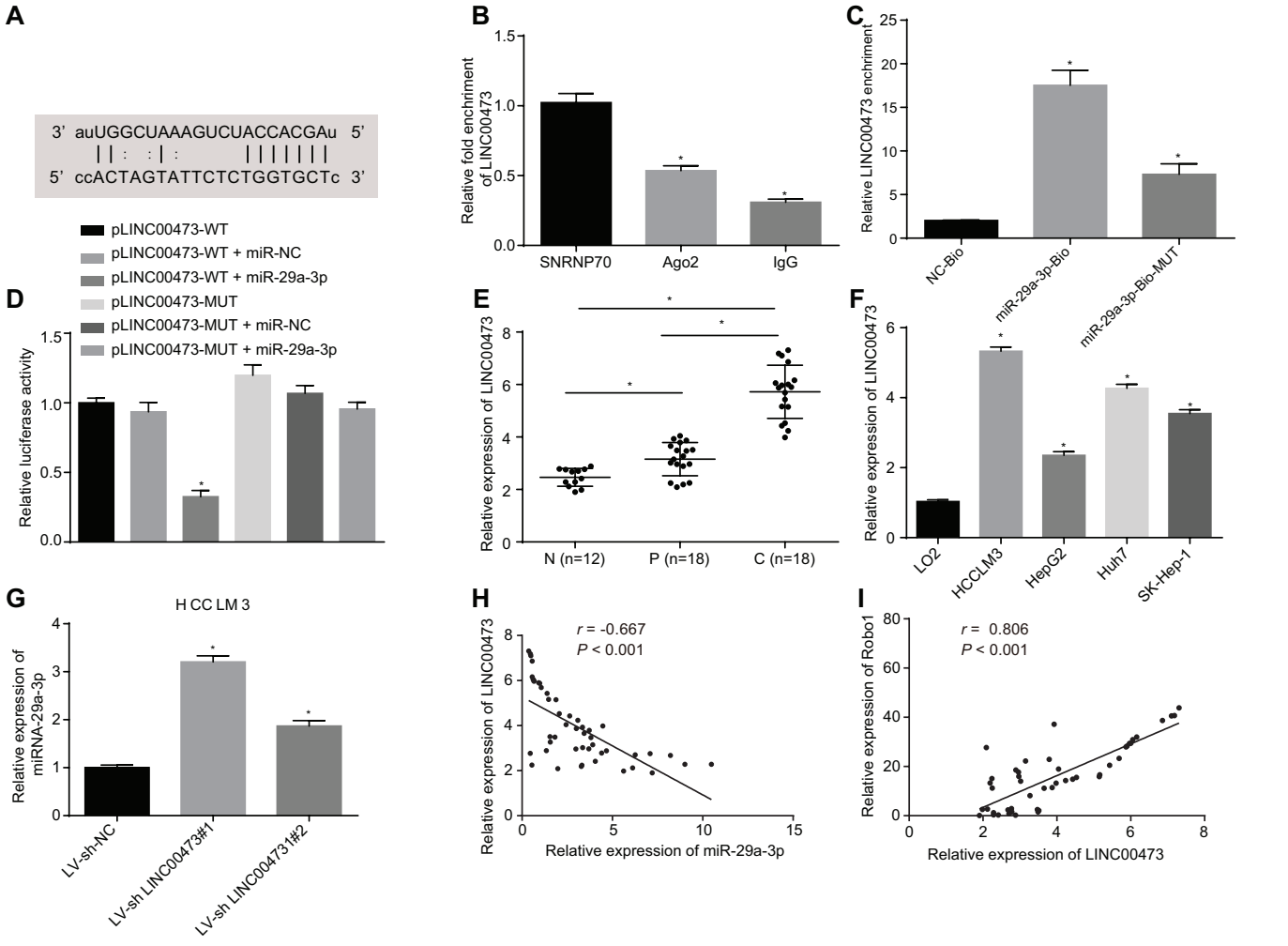

Figure 6. LINC00473 competitively bound to miR-29a-3p to upregulate Robo1 expression. (A) the binding site between LINC00473 and miR-29a-3p analyzed by the bioinformatics website (http://www.microrna.org); (B) the binding relationship between LINC00473 and miR-29a-3p examined by Ago2-RIP assay with IgG serving as a negative control and SNRNP70 as a positive control (*$p < 0.05$, compared with the SNRNP70 group); (C) the binding relationship between LINC00473 and miR-29a-3p in HCC-LM3 cells examined by RNA pull down assay (*$p < 0.05$, compared with the NC-Bio group); (D) the interaction between LINC00473 and miR-29a-3p examined by luciferase reporter gene assay (*$p < 0.05$, compared with the LINC00473-WT group); (E) the expression of LINC00473 in 18 cases of HCC tissues, 18 cases of paracancerous tissues and 12 cases of normal liver tissues determined by RT-qPCR; (F) the relative expression of LINC00473 in HCC-LM3 cell lines. *$p < 0.05$, compared with normal liver cell lines; $n = 3$; (G) the expression of miR-29a-3p in HCCLM3 cells examined by RT-qPCR (*$p < 0.05$, compared with the LV-sh group); (H) the relationship between miR-29a-3p and LINC00473 in HCC-LM3 cells examined by correlation analysis; (I) the relationship between LINC00473 and Robo1 determined by correlation analysis.
HCC, hepatocellular carcinoma; NC, negative control; RT-qPCR, reverse transcription quantitative polymerase chain reaction; WT, wild type.

conclusion, our findings demonstrated that miR-29-3p overexpression resulted in the inhibition of HCC cell proliferation, migration, invasion, and metastasis by inactivating the PI3K/AKT/mTOR signaling pathway *via* Robo1 downregulation and that LINC00473 might participate in HCC progression by acting as a ceRNA of miR-29a-3p.

The first observation was that Robo1 was highly expressed in HCC tissues and cells. Similar to our finding, another research reveals that Robo1 expresses at a high level in HCC, and its high expression may indicate its underlying role as a target protein for immunotherapy.[29] In addition, our study found that the silencing of Robo1 resulted in the inhibition of the proliferation, migration, and invasion of HCC cells and tumor growth. Robo1 plays an essential part in cell motility and migration during embryogenesis and organogenesis and in numerous primary tumors.[15] Robo1 has also been identified as a suppressor in both prostate and breast cancer and correlates

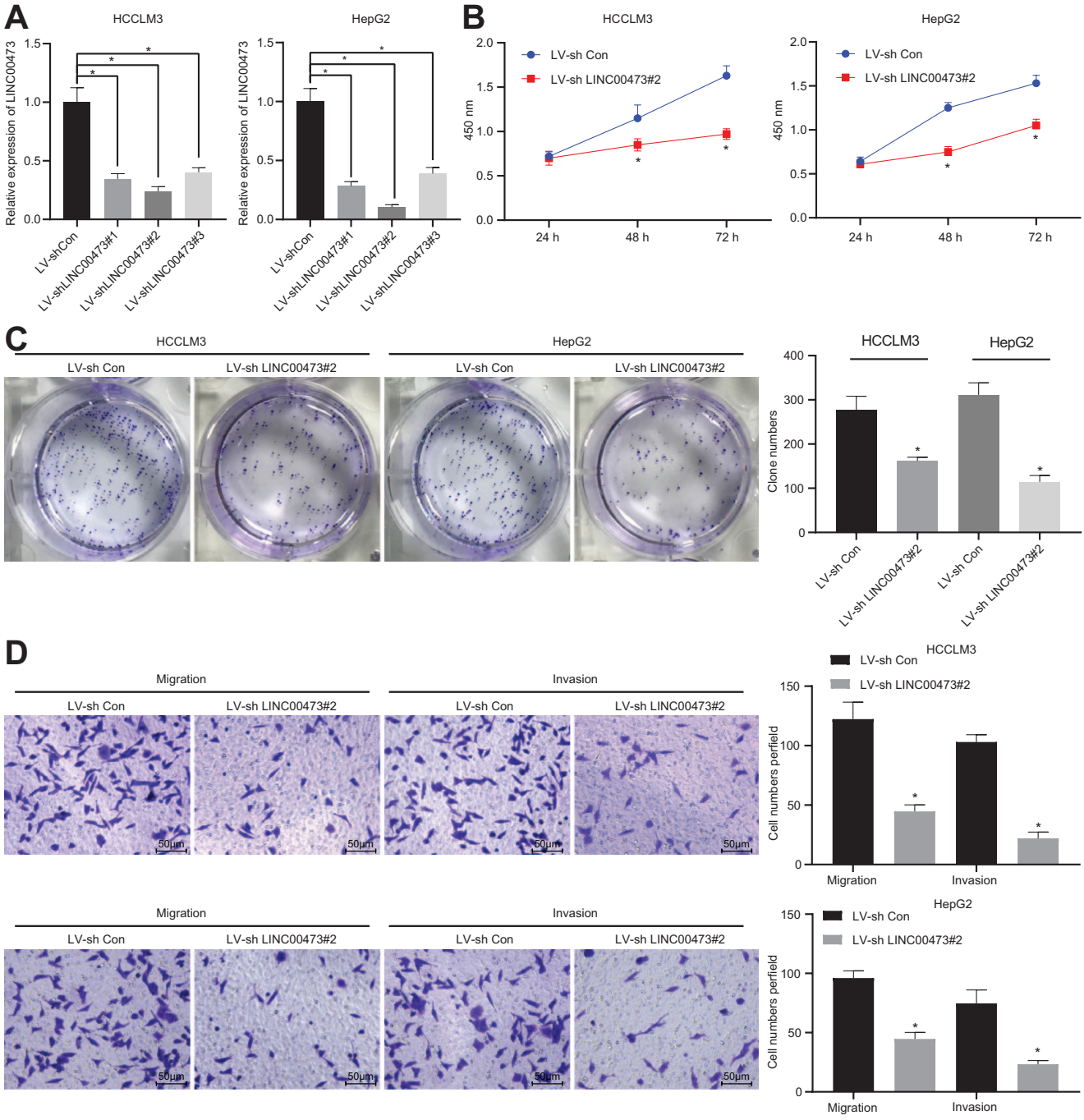

Figure 7. Silencing of LINC00473 restrains the proliferation, migration, and invasion of HCC cells. (A) LINC00473 expression in HCC cells infected with lentiviruses expressing sh-LINC00473#1, sh-LINC00473#2, and sh-LINC00473#3; (B) the proliferation of HCC cells examined by CCK-8 assay; (C) the number of clones of HCC cells examined by colony formation assay; (D) the migration and invasion of HCC cells measured by Transwell assay (200×). $^{*}p < 0.05$, compared with the LV-shCon group. $n = 3$. Data in panel A were analyzed by one-way ANOVA, panel B by repeated measures ANOVA and data in panel C, D were analyzed by unpaired t test.
ANOVA, analysis of variance; HCC, hepatocellular carcinoma; LV-sh, lentivirus short hairpin; RT-qPCR, reverse transcription quantitative polymerase chain reaction.

with an improved prognosis.[24] Moreover, Robo1 has been associated with tumor metastasis and angiogenesis in small cell lung cancer.[30] Slit2/Robo1 signaling has been shown to suppress tumor cell proliferation and migration in lung carcinogenesis and the Slit/Robo1 axis is involved

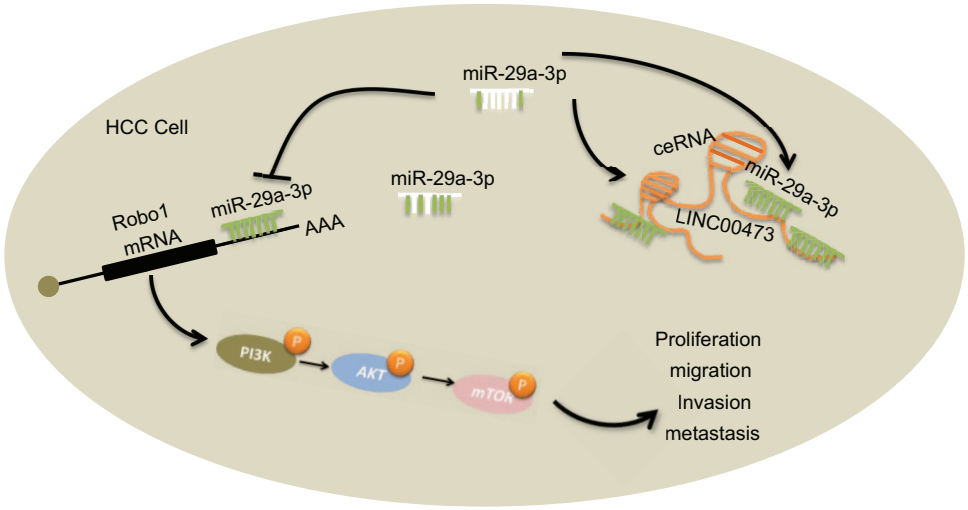

Figure 8. Schematic graph of the regulatory network of the LINC00473/miR-29-3p/Robo1 axis in HCC progression. miR-29a-3p negatively regulates Robo1 expression. LINC00473 could act as a ceRNA of miR-29a-3p to promote Robo1 expression, which results in augmented HCC cell proliferation, migration, invasion, and metastasis *via* activating the PI3K/AKT/mTOR signaling pathway.
ceRNA, competing endogenous RNAs; HCC, hepatocellular carcinoma.

in cancer pathogenesis of esophageal squamous cell carcinoma by mediating cell invasion.[31,32] Furthermore, our study showed that the role of Robo1 silencing in HCC was achieved through inactivation of the PI3K/AKT/mTOR signaling pathway. Consistent to our results, a prior study suggested that Robo1 inhibits PI3K/AKT pathway to suppress angiogenesis in diabetic nephropathy.[33] There is evidence showing that the PI3K/AKT/mTOR signaling pathway is frequently activated in HCC and its aberrant activation is correlated with poor HCC prognosis.[34]

Moreover, the poor expression of miR-29a-3p has been observed in HCC tissues and cells. miR-29 family members are frequently downregulated in diverse cancer types and therefore could be considered as potential tumor suppressors.[35] For instance, there is a reduction in miR-29a-3p expression in gastric cancer, which is known to exert tumor inhibitory function by suppressing cell growth and metastasis.[36] In addition, it was observed that elevation of miR-29a-3p resulted in the inhibition of tumorigenesis and metastasis *in vitro* as well as repressed tumor growth *in vivo* possibly *via* the inactivation of the PI3K/AKT/mTOR signaling pathway. Wang *et al.* also demonstrated that the overexpression of miR-29a-3p resulted in the suppression of HCC cell proliferation and migration, which further verifies miR-29a-3p as a tumor suppressor with critical functions in HCC tumorigenesis.[12] PI3K/AKT/mTOR signaling pathway was found to be activated in HCC, which is linked to HCC cell growth and apoptosis.[37] miR-29 is essential for the proliferation of human lung fibroblasts due to its ability to inactivate the PI3K/AKT signaling pathway.[38] Furthermore, Robo1 was verified to be a target gene of miR-29a-3p. Liu *et al.* suggested in their study that the dysregulation of Robo1 is related to a number of cancer types and its expression could be negatively regulated by miR-29a in gastric cancer cells.[39]

Dysregulation of lncRNAs has been reported to participate in the initiation and progression of different diseases *via* direct regulation of proteins or indirect regulation of miRNA-target genes.[8] The obtained results from the current study also revealed that LINC00473 could competitively bind to miR-29a-3p to upregulate Robo1 expression. lncRNAs can act as ceRNAs of miRNAs to reverse-mediate the expression of miRNAs.[40] A previous study showed that LINC005 promotes proliferation, invasion, and tumor angiogenesis in pancreatic ductal adenocarcinoma by acting as a sponge for miR-29b-3p.[41] LINC00473 also serves as an oncogene in HCC to promote proliferative and invasive abilities of HCC cells potentially *via* the mechanism of recruiting deubiquitinase USP9X to suppress survivin ubiquitination level.[7] Moreover, although overexpression of miR-195 results in the inhibition of survival and

metastasis of Wilms tumor, LINC00473 could counteract this inhibitory effect by binding to miR-195 to restrain its availability.[25] LINC00473 was found to competitively bind to miR-29a-3p to regulate Robo1 expression; however, further studies are required to elucidate the specific role of LINC00473 on HCC cell proliferation, migration, and invasion.

In conclusion, the current study unraveled the involvement of the LINC00473/miR-29-3p/Robo1 axis in the development of HCC (Figure 8). Upregulated miR-29-3p could inhibit HCC proliferation, migration, invasion, and metastasis through inhibition of Robo1 and inactivation of PI3K/Akt/mTOR signaling pathway. Meanwhile, LINC00473 could act as a miR-29-3p sponge to upregulate the Robo1 expression, which allows for a better understanding for the role of miR-29-3p and LINC00473 in hepatocarcinogenesis. Thus, miR-29a-3p may serve as a cancer suppressor and a potential therapeutic target of HCC. However, owing to the limitation of expenditure, more efforts should be done in future studies to elucidate the specific mechanisms by which LINC00473 influences the initiation and progression of HCC.

Acknowledgments

We thank Li-Yu Wang (Department of Hepatobiliary Surgery, Union Hospital, Tongji Medical College, Huazhong University of Science and Technology) for his technical assistance.

Conflict of interest statement

The authors declare that there is no conflict of interest.

Funding

The authors disclosed receipt of the following financial support for the research, authorship, and/or publication of this article: This work was supported by Schistosomiasis Control Project in Hubei Province (No. XF2012-17) and the National Science and Technology Major Project (No.2012ZX10005-005;No.2014ZX10005001).

ORCID iD

Jiaquan Huang https://orcid.org/0000-0001-9716-8958

Supplemental material

Supplemental material for this article is available online.

References

1. Huang JL, Zheng L, Hu YW, *et al.* Characteristics of long non-coding RNA and its relation to hepatocellular carcinoma. *Carcinogenesis* 2014; 35: 507–514.
2. Gao JZ, Li J, Du JL, *et al.* Long non-coding RNA HOTAIR is a marker for hepatocellular carcinoma progression and tumor recurrence. *Oncol Lett* 2016; 11: 1791–1798.
3. Liu Y, Pan S, Liu L, *et al.* A genetic variant in long non-coding RNA HULC contributes to risk of HBV-related hepatocellular carcinoma in a Chinese population. *PLoS One* 2012; 7: e35145.
4. Tu ZQ, Li RJ, Mei JZ, *et al.* Down-regulation of long non-coding RNA GAS5 is associated with the prognosis of hepatocellular carcinoma. *Int J Clin Exp Pathol* 2014; 7: 4303–4309.
5. Guo S, Chen W, Luo Y, *et al.* Clinical implication of long non-coding RNA NEAT1 expression in hepatocellular carcinoma patients. *Int J Clin Exp Pathol* 2015; 8: 5395–5402.
6. Liu YR, Tang RX, Huang WT, *et al.* Long noncoding RNAs in hepatocellular carcinoma: novel insights into their mechanism. *World J Hepatol* 2015; 7: 2781–2791.
7. Chen H, Yang F, Li X, *et al.* Long noncoding RNA LNC473 inhibits the ubiquitination of survivin via association with USP9X and enhances cell proliferation and invasion in hepatocellular carcinoma cells. *Biochem Biophys Res Commun* 2018; 499: 702–710.
8. Wang L, Zhang X, Sheng L, *et al.* LINC00473 promotes the Taxol resistance via miR-15a in colorectal cancer. *Biosci Rep* 2018; 38: BSR20180790.
9. Li B, Mao R, Liu C, *et al.* LncRNA FAL1 promotes cell proliferation and migration by acting as a CeRNA of miR-1236 in hepatocellular carcinoma cells. *Life Sci* 2018; 197: 122–129.
10. Wu L, Pan C, Wei X, *et al.* lncRNA KRAL reverses 5-fluorouracil resistance in hepatocellular carcinoma cells by acting as a ceRNA against miR-141. *Cell Commun Signal* 2018; 16: 47.
11. Gramantieri L, Ferracin M, Fornari F, *et al.* Cyclin G1 is a target of miR-122a, a microRNA frequently down-regulated in human hepatocellular carcinoma. *Cancer Res* 2007; 67: 6092–6099.
12. Wang X, Liu S, Cao L, *et al.* miR-29a-3p suppresses cell proliferation and migration by downregulating IGF1R in hepatocellular carcinoma. *Oncotarget* 2017; 8: 86592–86603.

13. Zhao Z, Wang L, Song W, *et al*. Reduced miR-29a-3p expression is linked to the cell proliferation and cell migration in gastric cancer. *World J Surg Oncol* 2015; 13: 101.

14. Seki M, Watanabe A, Enomoto S, *et al*. Human ROBO1 is cleaved by metalloproteinases and gamma-secretase and migrates to the nucleus in cancer cells. *FEBS Lett* 2010; 584: 2909–2915.

15. Parray A, Siddique HR, Kuriger JK, *et al*. ROBO1, a tumor suppressor and critical molecular barrier for localized tumor cells to acquire invasive phenotype: study in African-American and Caucasian prostate cancer models. *Int J Cancer* 2014; 135: 2493–2506.

16. Ao JY, Chai ZT, Zhang YY, *et al*. Robo1 promotes angiogenesis in hepatocellular carcinoma through the Rho family of guanosine triphosphatases' signaling pathway. *Tumour Biol* 2015; 36: 8413–8424.

17. Li Y, Fu S, Chen H, *et al*. Inhibition of endothelial Slit2/Robo1 signaling by thalidomide restrains angiogenesis by blocking the PI3K/Akt pathway. *Dig Dis Sci* 2014; 59: 2958–2966.

18. Jiang W, Zhang W, Wu L, *et al*. MicroRNA-related polymorphisms in PI3K/Akt/mTOR pathway genes are predictive of limited-disease small cell lung cancer treatment outcomes. *Biomed Res Int* 2017; 2017: 6501385.

19. Gedaly R, Angulo P, Hundley J, *et al*. PI-103 and sorafenib inhibit hepatocellular carcinoma cell proliferation by blocking Ras/Raf/MAPK and PI3K/AKT/mTOR pathways. *Anticancer Res* 2010; 30: 4951–4958.

20. Jia JB, Wang WQ, Sun HC, *et al*. High expression of macrophage colony-stimulating factor-1 receptor in peritumoral liver tissue is associated with poor outcome in hepatocellular carcinoma after curative resection. *Oncologist* 2010; 15: 732–743.

21. Zhang Y, Liu H, Li W, *et al*. CircRNA_100269 is downregulated in gastric cancer and suppresses tumor cell growth by targeting miR-630. *Aging (Albany NY)* 2017; 9: 1585–1594.

22. Gong T, Ning X, Deng Z, *et al*. Propofol-induced miR-219-5p inhibits growth and invasion of hepatocellular carcinoma through suppression of GPC3-mediated WNT/beta-catenin signalling activation. *J Cell Biochem* 2019; 120: 16934-16945.

23. He C, Liu Z, Jin L, *et al*. lncRNA TUG1-mediated Mir-142-3p downregulation contributes to metastasis and the epithelial-to-mesenchymal transition of hepatocellular carcinoma by targeting ZEB1. *Cell Physiol Biochem* 2018; 48: 1928–1941.

24. Chang PH, Hwang-Verslues WW, Chang YC, *et al*. Activation of Robo1 signaling of breast cancer cells by Slit2 from stromal fibroblast restrains tumorigenesis via blocking PI3K/Akt/beta-catenin pathway. *Cancer Res* 2012; 72: 4652–4661.

25. Zhu S, Fu W, Zhang L, *et al*. LINC00473 antagonizes the tumour suppressor miR-195 to mediate the pathogenesis of Wilms tumour via IKKalpha. *Cell Prolif* 2018; 51: e12416.

26. Calvisi DF, Ladu S, Gorden A, *et al*. Ubiquitous activation of RAS and JAK/STAT pathways in human HCC. *Gastroenterology* 2006; 130: 1117–1128.

27. Zhou J, Yu L, Gao X, *et al*. Plasma microRNA panel to diagnose hepatitis B virus-related hepatocellular carcinoma. *J Clin Oncol* 2011; 29: 4781–4788.

28. Tsai WC, Hsu PW, Lai TC, *et al*. MicroRNA-122, a tumor suppressor microRNA that regulates intrahepatic metastasis of hepatocellular carcinoma. *Hepatology* 2009; 49: 1571–1582.

29. Fujiwara K, Koyama K, Suga K, *et al*. A (90) Y-labelled anti-ROBO1 monoclonal antibody exhibits antitumour activity against hepatocellular carcinoma xenografts during ROBO1-targeted radioimmunotherapy. *EJNMMI Res* 2014; 4: 29.

30. Fujiwara K, Koyama K, Suga K, *et al*. 90Y-labeled Anti-ROBO1 monoclonal antibody exhibits antitumor activity against small cell lung cancer xenografts. *PLoS One* 2015; 10: e0125468.

31. Wang Y, Zhang S, Bao H, *et al*. MicroRNA-365 promotes lung carcinogenesis by downregulating the USP33/SLIT2/ROBO1 signalling pathway. *Cancer Cell Int* 2018; 18: 64.

32. Jiang L, Wang Y, Rong Y, *et al*. miR-1179 promotes cell invasion through SLIT2/ROBO1 axis in esophageal squamous cell carcinoma. *Int J Clin Exp Pathol* 2015; 8: 319–327.

33. Liu J, Hou W, Guan T, *et al*. Slit2/Robo1 signaling is involved in angiogenesis of glomerular endothelial cells exposed to a diabetic-like environment. *Angiogenesis* 2018; 21: 237–249.

34. Wang X, Han L, Zhang J, *et al*. Down-regulated NRSN2 promotes cell proliferation and survival through PI3K/Akt/mTOR pathway in hepatocellular carcinoma. *Dig Dis Sci* 2015; 60: 3011–3018.

35. Dong CW, Wang YX, Du FT, *et al*. Low miR-29c expression is a prognostic marker in hepatocellular carcinoma. *Genet Mol Res* 2016; 15.

36. Bai F, Jiu M, You Y, *et al*. miR29a3p represses proliferation and metastasis of gastric cancer cells via attenuating HAS3 levels. *Mol Med Rep* 2018; 17: 8145–8152.

37. Hong SW, Jung KH, Lee HS, *et al*. SB365 inhibits angiogenesis and induces apoptosis of hepatocellular carcinoma through modulation of PI3K/Akt/mTOR signaling pathway. *Cancer Sci* 2012; 103: 1929–1937.

38. Yang T, Liang Y, Lin Q, *et al*. miR-29 mediates TGFbeta1-induced extracellular matrix synthesis through activation of PI3K-AKT pathway in human lung fibroblasts. *J Cell Biochem* 2013; 114: 1336–1342.

39. Liu X, Cai J, Sun Y, *et al*. MicroRNA-29a inhibits cell migration and invasion via targeting Roundabout homolog 1 in gastric cancer cells. *Mol Med Rep* 2015; 12: 3944–3950.

40. Chen DL, Lu YX, Zhang JX, *et al*. Long non-coding RNA UICLM promotes colorectal cancer liver metastasis by acting as a ceRNA for microRNA-215 to regulate ZEB2 expression. *Theranostics* 2017; 7: 4836–4849.

41. Zhao X, Liu Y, Li Z, *et al*. Linc00511 acts as a competing endogenous RNA to regulate VEGFA expression through sponging hsa-miR-29b-3p in pancreatic ductal adenocarcinoma. *J Cell Mol Med* 2018; 22: 655–667.